Draft version May 3, 2013
Preprint typeset using LaTeX style emulateapj v. 5/2/11

arXiv:1305.0276v1 [astro-ph.GA] 1 May 2013

CONSTRAINT ON THE POLARIZATION OF ELECTRIC DIPOLE EMISSION FROM SPINNING DUST

Thiem Hoang[1], A. Lazarian[2], and P. G. Martin[1]

Draft version May 3, 2013

ABSTRACT

Planck results have revealed that the electric dipole emission from polycyclic aromatic hydrocarbons (PAHs) is the most likely explanation for anomalous microwave emission that interferes with cosmic microwave background (CMB) radiation experiments. The emerging question is to what extent this emission component contaminates to the polarized CMB radiation. We present constraints on polarized dust emission for the model of grain size distribution and grain alignment that best fits to observed extinction and polarization data. Two stars with a prominent polarization excess at $\lambda = 2175$ Å, HD 197770 and HD 147933-4, are chosen for our study. For HD 197770, we find that the model with aligned silicate grains plus weakly aligned PAHs can reproduce the 2175 Å polarization feature; whereas, for HD 147933-4, we find that the alignment by silicate grains only can account for that feature. The alignment function of PAHs for the best fit model to the HD 197770 data is employed to constrain polarized spinning dust emission. We find that the degree of polarization of spinning dust emission is about 3.2% at frequency $\nu = 5$ GHz and rapidly declines to below 1.8% for $\nu > 20$ GHz. We also predict the degree of polarization of thermal dust emission at 353 GHz to be $P_{\rm em} = 9.9\%$ and 14.5% for the HD 197770 and HD 147933-4 stars, respectively.

Subject headings: cosmic microwave background–diffuse radiation–dust, extinction–radiation mechanisms:non-thermal

1. INTRODUCTION

Cosmic Microwave Background (CMB) experiments (see Bouchet et al. 1999; Tegmark et al. 2000; Efstathiou 2003; Bennett et al. 2003) are of great importance for studying the early universe and its subsequent expansion. Precision cosmology with *Wilkinson Microwave Anisotropy Probe* (*WMAP*) and *Planck* requires a good model of the microwave foreground emission to allow the reliable subtraction of foreground contamination from the CMB radiation.

In the 10–60 GHz frequency range, electric dipole emission (Draine & Lazarian 1998) from rapidly spinning tiny dust grains (mostly polycyclic aromatic hydrocarbons, hereafter PAHs) is an important component of Galactic foregrounds that dominates the CMB signal (see Planck Collaboration et al. 2013b). In the last several years, significant progress has been made in understanding spinning dust in terms of both theory (Ali-Haïmoud et al. 2009; Hoang et al. 2010; Hoang et al. 2011; Silsbee et al. 2011; see Hoang & Lazarian 2012 for a review) and observation (Dickinson et al. 2009; Kogut et al. 2011; Tibbs et al. 2012). In particular, *Planck* results have confirmed spinning dust emission as the most reliable source of anomalous microwave emission (AME) (Planck Collaboration et al. 2011). *Planck* is poised to release interesting results on the CMB polarization; however, the question to what extent the spinning dust emission contaminates to the polarized CMB signal remains unclear.

The degree of polarization of spinning dust emission depends on how efficient the alignment of PAHs is in the interstellar magnetic field. Lazarian & Draine (2000) (hereafter LD00) suggested that PAHs can be aligned via resonance paramagnetic relaxation–a mechanism which extends the classical Davis-Greenstein (Davis & Greenstein 1951) mechanism for very fast rotating grains for which the Barnett magnetization arising from fast rotation of grains cannot be neglected. They predicted the polarization of spinning dust typically $\leq 1\%$ for frequency $\nu > 20$ GHz.

Recent observational studies (López-Caraballo et al. 2011; Macellari et al. 2011 showed that the upper limit for the AME polarization is between $2 - 5\%$. In addition, an upper limit of 1% for the AME polarization is reported in various media (see Rubiño-Martín et al. 2012). Since *Planck* and other CMB experiments provide extremely precise measurements of polarization, a reliable prediction for the spinning dust polarization is useful for separation of polarized Galactic foreground components from the CMB.

The problem of grain alignment, especially for PAHs[3] is complicated in general (see Lazarian 2007 for a review), but one can derive constraints on grain alignment observationally (see Martin 2007). An important attempt to obtain observational constraints on grain alignment was carried out in a classical paper by Kim & Martin (1995). The authors applied maximum entropy method to infer the mass distribution of aligned grains through fitting theoretical polarization curves to observation data. They discovered that interstellar silicate grains of size $a \geq 0.05\,\mu$m are aligned, whereas smaller grains, including PAHs, are weakly aligned. Draine & Fraisse (2009) performed simultaneous fitting to the typical extinction and polarization curve of the diffuse ISM and came to

---

[1] Canadian Institute for Theoretical Astrophysics, University of Toronto, 60 St. George Street, Toronto, ON M5S 3H8, Canada
[2] Department of Astronomy, University of Wisconsin-Madison, Madison, WI 53705, USA

[3] The accepted theory of grain alignment for large grains is that based on radiative torques (Dolginov & Mitrofanov 1976; Draine & Weingartner 1996, Draine & Weingartner 1997; Lazarian & Hoang 2007, Lazarian & Hoang 2008; Hoang & Lazarian 2008, Hoang & Lazarian 2009b, Hoang & Lazarian 2009a) but the radiative torques are negligibly small for PAHs. This encourages us to explore the possibilities provided by other alignment mechanisms.

the similar conclusion as in Kim & Martin (1995) that small ($a < 0.05\,\mu$m) grains are weakly aligned and large ($a > 0.1\,\mu$m) grains are efficiently aligned.

Since the tiny dust grains that radiate spinning dust emission are likely the same as those that induce the ultraviolet (UV) extinction bump at $\lambda = 2175$Å,[4] a natural way to search for the alignment of PAHs is through its imprint on the UV polarization. While the UV extinction bump is ubiquitous in the diffuse interstellar medium (ISM), the UV polarization bump is rarely seen, except for two stars HD 197770 and HD147933-4, which show a prominent UV polarization feature at $\lambda = 2175$Å (Clayton et al. 1992; Wolff et al. 1993; Wolff et al. 1997). In addition to the UV polarization excess, HD 197770 exhibits a polarization plateau that cannot be accounted for with the typical ISM polarization curve–Serkowski law (Serkowski 1973).

A number of studies have suggested that the UV polarization bump can arise from aligned small graphite grains (Draine 1988; Wolff et al. 1993; Wolff et al. 1997); however, a detailed study on the alignment efficiency of small graphite grains is not yet available.

The main goal of this paper is to find the degree of alignment of interstellar grains including PAHs that reproduces the UV polarization excess seen in HD 197770 and HD 147933-4 and employ the inferred degree of alignment to predict the degree of polarization of spinning dust emission. The paper is structured as follows.

In §2 we calculate extinction cross section and polarization cross section for silicate and carbonaceous oblate spheroidal grains. In §3, we describe a procedure to derive grain size distributions and degree of grain alignment by fitting theoretical predictions to observed extinction and polarization curves and present the obtained results. In §4 polarized spinning dust emission is calculated using the degree of grain alignment obtained for the best fit model. Discussion and summary are presented in §5 and §6, respectively.

2. OPTICAL PROPERTIES OF DUST GRAINS

2.1. *Extinction and Polarization Cross Section*

Interstellar dust grains are widely known to induce the extinction and polarization of starlight due the absorption and scattering of light out of the line of sight by dust grains.

Let us consider an oblate spheroidal grain with the symmetry axis $\mathbf{a}_1$. A perfectly polarized electromagnetic wave with the electric field vector $\mathbf{E}$ propagates along the $\hat{\mathbf{z}}$ direction, which is perpendicular to the symmetry axis. Let $C_{\rm ext}(\mathbf{E}\perp\mathbf{a}_1)$ and $C_{\rm ext}(\mathbf{E}\|\mathbf{a}_1)$ be the extinction of radiation for the cases in which $\mathbf{E}$ is parallel and perpendicular to $\mathbf{a}_1$, respectively. For the sake of simplification, we denote these extinction cross sections by $C_\perp$ and $C_\|$.

For the general case in which $\mathbf{E}$ makes an angle θ with $\mathbf{a}_1$, the extinction cross section becomes

$$C_{\rm ext} = \cos^2\theta C_\| + \sin^2\theta C_\perp, \quad (1)$$

Since the original starlight is unpolarized, one can compute the total extinction cross section for a randomly oriented grain by integrating Equation (1) over the isotropic distribution of θ, i.e., $f_{\rm iso}d\theta \sim \sin\theta d\theta$. As a result,

$$C_{\rm ext} = \frac{1}{3}\left(2C_\perp + C_\|\right). \quad (2)$$

The dust extinction cross section can be represented through the extinction efficiency, which is defined as the ratio of the extinction cross section to the geometrical cross section:

$$Q_{\rm ext}(a,\lambda) = \frac{C_{\rm ext}(a,\lambda)}{\pi a^2}. \quad (3)$$

The polarization coefficient for oblate spheroidal grains is equal to

$$C_{\rm pol} = \left[C_{\rm ext}(\mathbf{E}\|\mathbf{a}_1) - C_{\rm ext}(\mathbf{E}\perp\mathbf{a}_1)\right]. \quad (4)$$

2.2. *Silicate grains*

For silicate grains, we adopt the DDSCAT code (Draine & Flatau 2012) to compute the extinction cross section $C_{\rm ext}^{\rm sil}(a,\lambda)$ using the dielectric functions of amorphous silicate from Draine (2003).

Figure 1 shows $\lambda Q_{\rm ext}/a$ and $\lambda Q_{\rm pol}/a$ as functions of λ^{-1} for a silicate spheroidal grain with the axis ratio $a/b = 2$ and for the different grain sizes.

2.3. *Carbonaceous grains*

Carbonaceous grains consist of a fraction $\zeta_{\rm PAH}$ of PAHs and $1-\zeta_{\rm PAH}$ of graphite grains with

$$\zeta_{\rm PAH}(a) = (1-q_{\rm gra})\times\min\left[1,(a_\zeta/a)^3\right], \quad (5)$$

where $a_\zeta = 50$Å, $q_{\rm gra} = 0.01$ are assumed as in Draine & Li (2007).

For graphite grains, which are an anisotropic material, we assume the dielectric function from Draine (2003) and compute $C_{\rm ext}^{\rm gra}(a,\lambda)$ using DDSCAT. We consider two cases in which $\mathbf{E}$ are parallel and perpendicular to the grain optical axis (c-axis). Using the $\frac{1}{3}-\frac{2}{3}$ approximation, one can obtain the extinction cross section $C_{\rm ext}^{\rm gra} = \left(C_{\rm ext}(\mathbf{E}\|c) + 2C_{\rm ext}(\mathbf{E}\perp c)\right)/3$ for randomly oriented graphite grains.

For PAHs, the extinction $C_{\rm ext}^{\rm PAH}(\lambda)$ is computed as in Equations (5)-(10) in Li & Draine (2001). The polarization cross section of PAHs is taken to be the same as graphite grains of the same size.

2.4. *Extinction and Polarization Curve*

The extinction induced by randomly oriented grains in units of magnitude is defined by

$$\begin{aligned} A(\lambda) &= 2.5\log_{10}\left(\frac{F_\lambda^{\rm obs}}{F_\lambda^\star}\right) = 1.086\tau_\lambda, \\ &= 1.086\sum_{j=\rm carb,sil}\sum_{i=0}^{N_a-1} C_{\rm ext}^j(a_i)n^j(a_i)dz, \end{aligned} \quad (6)$$

where $F_\lambda^\star$ is the intrinsic flux from the star, $F_\lambda^{\rm obs} = F_\lambda^\star e^{-\tau_\lambda}$ is the observed flux, and τ_λ is the optical depth.

To find the polarization by aligned grains, let us define an observer's coordinate system in which the line of sight is directed along the $z-$axis, and $x-$ and $y-$ axes constitute the sky plane. The polarization of starlight

---

[4] Such a UV bump is believed to arise from the electronic transition $\pi-\pi^*$ in the sp^2-bonded carbon sheets of small carbonaceous grains (see Draine 1989; Draine & Li 2007).

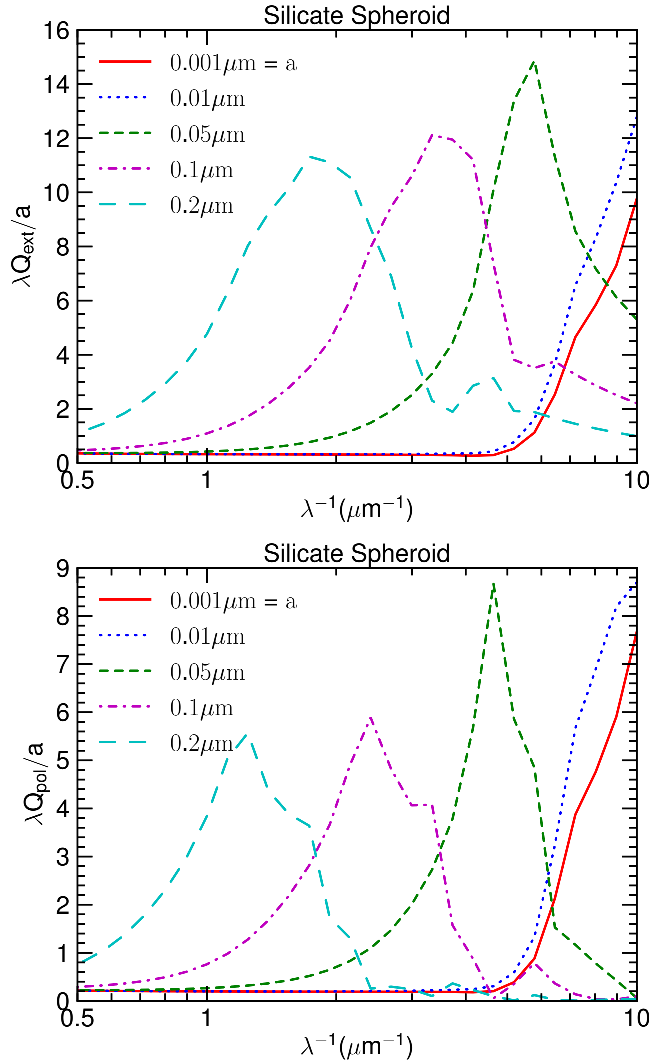

Fig. 1.— Extinction efficiency $\lambda Q_{\rm ext}/a$ (upper) and polarization efficiency $\lambda Q_{\rm pol}/a$ (lower) of silicate grains as functions of $1/\lambda$ for the different grain sizes.

arising from the dichroic extinction by aligned grains in a cell of dz is computed as

$$dp(\lambda) = \frac{d\tau_x - d\tau_y}{2} = \sum_{i=0}^{N_a-1} \frac{1}{2}\left(C_x - C_y\right) n(a_i) dz, \quad (7)$$

where N_a is the number of size bin, $n(a_i) \equiv (dn/da)da$ is the number of grains of size a_i, C_x and C_y are the grain cross section along $x-$ and $y-$ axes, respectively.

For the case of perfect internal alignment of grain symmetry axis $\mathbf{a}_1$ with angular momentum, by transforming the grain coordinate system to the observer's coordinate system and taking corresponding weights, we obtain

$$C_x = C_\perp - \frac{C_{\rm pol}}{2}\sin^2\beta, \quad (8)$$

$$C_y = C_\perp - \frac{C_{\rm pol}}{2}(2\cos^2\beta\cos^2\gamma + \sin^2\beta\sin^2\gamma), \quad (9)$$

where γ is the angle between the magnetic field and the sky plane and β is the angle between the grain angular momentum and the magnetic field.

The polarization efficiency then becomes

$$C_x - C_y = C_{\rm pol}\frac{\left(3\cos^2\beta - 1\right)}{2}\cos^2\gamma, \quad (10)$$

Taking the average of $C_x - C_y$ over the distribution of the alignment angle β, it yields

$$C_x - C_y = C_{\rm pol} Q_J \cos^2\gamma, \quad (11)$$

where $Q_J = \langle G_J \rangle$ is the ensemble average of $G_J = \left(3\cos^2\beta - 1\right)/2$ that describes the alignment of grain angular momentum with the ambient magnetic field.

When the internal alignment is not perfect, following the similar procedure, we obtain

$$C_x - C_y = C_{\rm pol}\langle G_J G_X \rangle \cos^2\gamma \equiv C_{\rm pol} R \cos^2\gamma, \quad (12)$$

where $G_X = \left(3\cos^2\theta - 1\right)/2$ with θ being the angle between grain symmetry axis and the angular momentum, and $R = \langle G_J G_X \rangle$ is the Rayleigh reduction factor (see also Roberge & Lazarian 1999). The degree of internal alignment is described by $Q_X = \langle G_X \rangle$.

For a perpendicular magnetic field, i.e., $\mathbf{B}$ lies on the sky plane, Equation (12) simply becomes $C_x - C_y = C_{\rm pol} R$.

Plugging Equation (12) into this above equation, we obtain

$$p(\lambda) = \sum_{j={\rm carb,sil}} \sum_{i=0}^{N_a-1} \frac{1}{2} C_{\rm pol}^j(a_i) R^j(a_i) n^j(a_i) dz, \quad (13)$$

where $R^j(a_i)$ is the Rayleigh reduction factor for the grain specie j of size a_i. In the following, the Rayleigh reduction factor can also be referred as the alignment function.

Frequently, it is more convenient to represent the extinction (polarization) through the extinction (polarization) cross section. Hence, the above equations can be rewritten as

$$A(\lambda) = 1.086\ \sigma_{\rm ext}(\lambda) \times N_{\rm H}, \quad (14)$$

$$p(\lambda) = \sigma_{\rm pol}(\lambda) \times N_{\rm H}, \quad (15)$$

where $N_{\rm H}(\,{\rm cm}^{-2})$ is the column density and $\sigma_{\rm ext}$ and $\sigma_{\rm pol}$ in units of ${\rm cm}^2{\rm H}^{-1}$ are the dust extinction cross section and polarization cross section, respectively.

3. GRAIN SIZE DISTRIBUTION AND GRAIN ALIGNMENT FUNCTION CONSTRAINED BY OBSERVATION

3.1. *Fitting method*

In this section, we find grain size distributions and alignment functions by fitting theoretical predictions to the observation data for the HD 197770 and HD 147933-4 stars. The parameters for these stars, including E_{B-V}, optical depth τ_V, the ratio of visual to selective extinction $R_V = A_V/E_{B-V}$, maximum polarization $p_{\rm max}$ and the wavelength at the peak $\lambda_{\rm max}$ are listed in Table 1 (see also Wolff et al. 1997).

We adopt the mixture dust model consisting of amorphous silicate grains, graphite grains and PAHs (see Weingartner & Draine 2001 ; Draine & Li 2007). We note that the grain size distribution may not be unique. For example, Draine & Fraisse (2009) obtained four different models of grain size distribution that can reproduce the diffuse ISM extinction and polarization data.

TABLE 1
Optical extinction and polarization parameters

Star	E_{B-V}	R_V	τ_V	$\lambda_{\rm max}(\mu{\rm m})$	$p_{\rm max}(\%)$
HD 197770	0.58	3.1	1.66	0.511 ± 0.001	3.90 ± 0.01
HD 147933-4	0.47	4.3	1.86	0.683 ± 0.003	2.72 ± 0.01

In the present paper, we assume that graphite grains of oblate spheroidal shape are randomly oriented. Such an assumption allows us to obtain an upper limit on the alignment efficiency of PAHs since aligned graphite grains would contribute some polarization to the 2175Å feature. We consider a model in which both silicate grains and PAHs are oblate spheroidal. The axis ratio $a/b = 2$ is adopted for the spheroidal grains as in the previous section. As in Draine & Fraisse (2009), we simultaneously fit theoretical predictions to the extinction curve and polarization curve.

Following Kim & Martin (1995), we find the grain size distribution and alignment function by minimizing χ^2, which is given by

$$\chi^2 = \chi^2_{\rm ext} + \chi^2_{\rm pol}, \qquad (16)$$

where

$$\chi^2_{\rm ext} = w_{\rm ext} \sum_{i=0}^{N_\lambda - 1} \left[A_{\rm mod}(\lambda_i) - A_{\rm obs}(\lambda_i)\right]^2, \qquad (17)$$

$$\chi^2_{\rm pol} = w_{\rm pol} \sum_{i=0}^{N_\lambda - 1} \left[p_{\rm mod}(\lambda_i) - p_{\rm obs}(\lambda_i)\right]^2, \qquad (18)$$

with $w_{\rm ext}$ and $w_{\rm pol}$ being the fitting weights for the extinction and polarization, respectively. Here, the summation is performed over N_λ wavelength bins. We consider $N_a = 128$ size bins from $a = 3.6$Å to $1\,\mu$m and $N_\lambda = 64$ from $\lambda = 0.15$ to $2.5\,\mu$m.

In the above equations, the observed extinction $A_{\rm obs}$ is calculated using the formula in Cardelli et al. (1989) when R_V is known, and $p_{\rm obs}$ is obtained from Wolff et al. (1997). The extinction $A_{\rm mod}(\lambda)$ and polarization $p_{\rm mod}(\lambda)$ are given by Equations (6) and (13). Following Draine & Allaf-Akbari (2006), we also introduce the constraints for the non-smoothness of the grain size distribution and alignment function.

The fitting procedure is started with an initial size distribution $n(a)$ that best reproduces the observational data for the diffuse ISM, which corresponds to model 3 in Draine & Fraisse (2009). By doing so, we implicitly assume that dust properties are similar throughout the ISM and the difference in the polarization of starlight is mainly due to the efficiency of grain alignment, which depends on environment conditions along the line of sight, e.g., radiation field, magnetic fields and gas density. For silicate grains, we take the alignment function for the ISM from Draine & Fraisse (2009) as an initial alignment function. For PAHs, we consider two cases. In the first case, we take the initial alignment function to be equal to that of silicate grains. In the second case, we assume an initial alignment function with a peak at $a = 10$Å from the theoretical prediction based on resonance paramagnetic alignment (see Hoang et al. 2013).

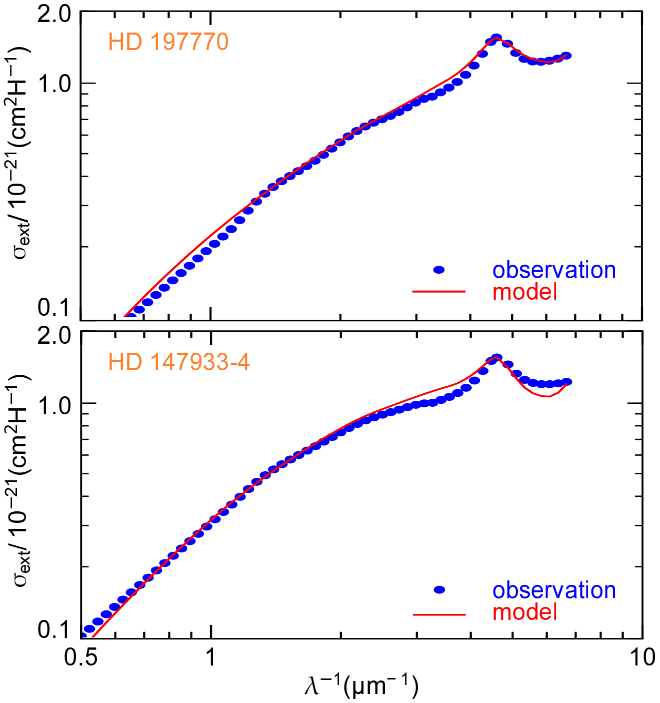

Fig. 2.— Observed extinction curve (filled ellipses) versus model for HD 197770 and HD 147933-4. An excellent fit achieved for HD 197770.

The fitting is carried out by the least square method based on Monte Carlo simulations. Basically, for each size bin, we add a small amount δR and δn generated from a uniform distribution to $R(a)$ and $n(a)$. Then, we calculate $A_{\rm mod}$ and $p_{\rm mod}$ for the new degree of alignment and size distribution using Equations (6) and (13). The value of χ^2 is also calculated. This sampling process is iterated for $N_{\rm rand} = 100$ times with each size bin to find the minimum χ^2.

3.2. *Results*

Figure 2 shows the extinction curves from our model compared to the observed data for the HD 197770 and HD 147933-4 stars. The model can reproduce the observed extinction of HD 197770 very well. For HD 147933-4, the model underestimates the extinction for $\lambda = 0.17 - 0.2\,\mu$m.

Figure 3 shows the mass distributions of silicate and carbonaceous grains for the best fit model for HD 197770 (upper) and HD 1479333-4 (lower). The distribution functions (DL07 and DF09) from Draine & Li (2007) and Draine & Fraisse (2009) are shown for comparison.

For HD 197770 with $R_V = 3.1$, it can be seen that the mass of PAHs in our model is the same as DL07 and DF09. The mass distribution of graphite grains is slightly different from DF09 for $a = 0.04 - 0.08\,\mu$m, but it is distinct from DL07. For silicate grains, the mass distribution peaks at $a \approx 0.07\,\mu$m. Compared to DF09, our model requires a slight increase of silicate mass to account for the polarization plateau seen in HD 197770.

For HD 147933-4 with $R_V = 4.3$, the mass distribution of silicate grains peaks at a larger size ($a \approx 0.25\,\mu$m) than for HD 197770, whereas the mass of $0.03 - 0.2\,\mu$m silicate

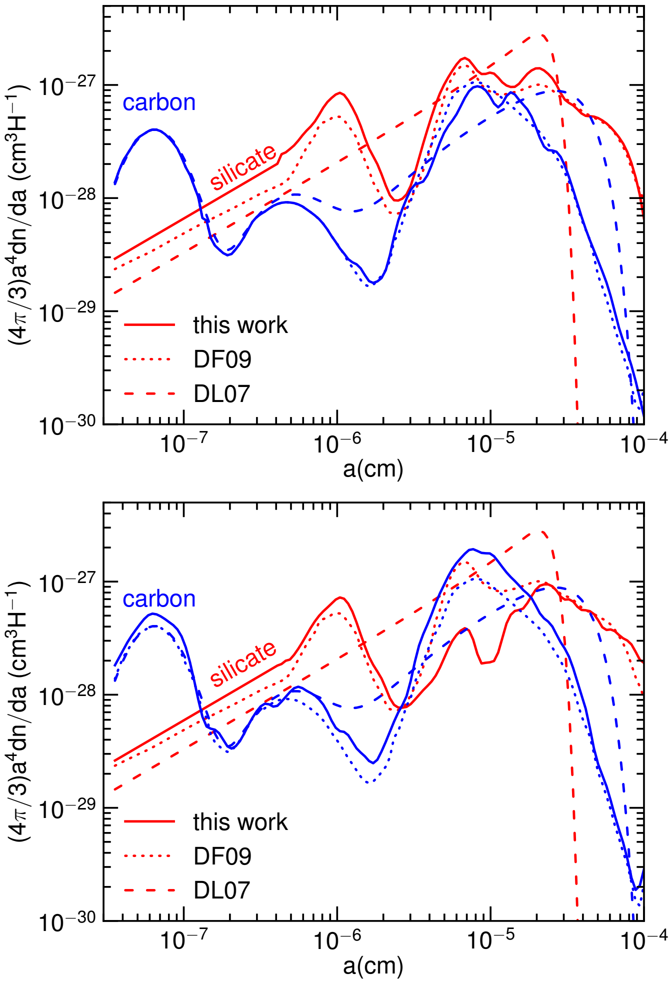

FIG. 3.— Mass distribution of silicate grains and carbonaceous grains for the best fit model (solid lines) for the HD 197770 (upper) and HD 147933-4 (lower) stars. Dotted (DF09) and dashed (DL07) lines show the grain mass distributions from Draine & Fraisse (2009) and Draine & Li (2007).

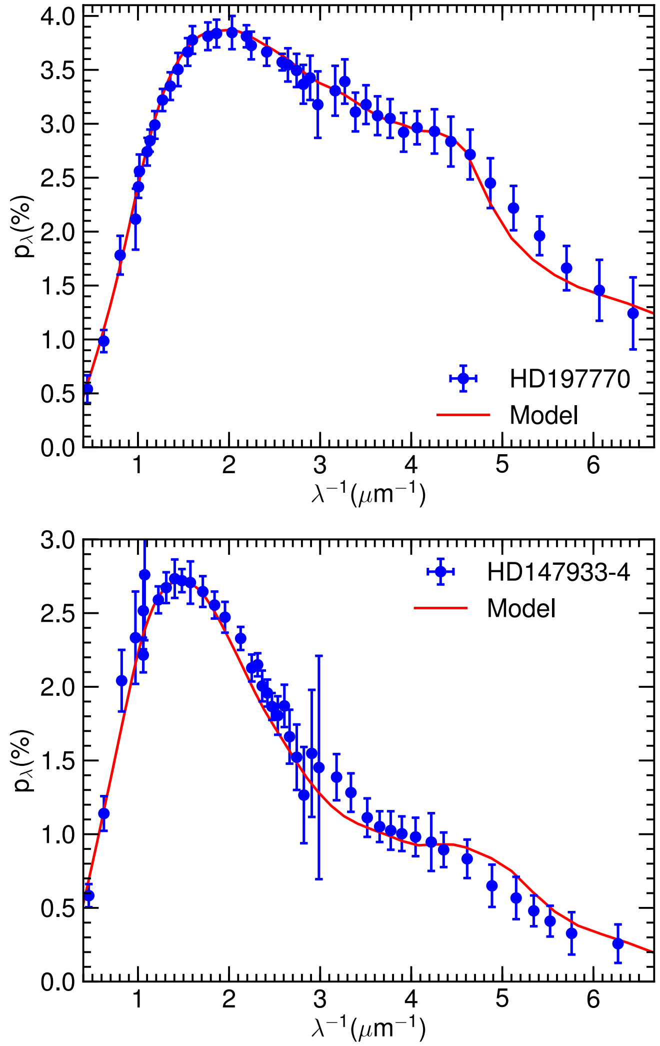

FIG. 4.— Polarization curves for our model versus the observed polarization data for HD 197770 (upper) and HD 147933-4 (lower). The 3σ error bars are shown.

grains is reduced. The peak in the mass of ($\sim 0.08\,\mu$m) graphite grains is also increased compared to DF09. Such a decrease in the mass of small grains and increase in the mass of large grains is necessary to reproduce the value of R_V higher than the typical value ($R_V = 3.1$) of the diffuse ISM.

Figure 4 shows the best fit model versus the observed polarization data from Wolff et al. (1997). Here we show the error bars of 3σ. For HD 197770, it can be seen that the model reproduces the 2175 Å polarization feature very well. The UV polarization bump in HD 147933-4 can also be accounted for, but the model shows a broad bump from $\lambda^{-1} = 4.0 - 5.8\,\mu$m^{-1} around the 2175Å feature.

Figure 5 (upper) shows the alignment function $R(a)$ that reproduces the polarization curve in Figure 4 for HD 197770. We can see that the alignment of silicate grains rises rapidly from $a = 0.06\,\mu$m and becomes constant with $R = 0.46$ for $a > 0.2\,\mu$m. For $a < 0.06\,\mu$m, the degree of alignment declines more or less smoothly with the increasing a but is still considerable ($R(a) = 0.01 - 0.05$) for very small silicate grains of $a = 0.003 - 0.06\,\mu$m. The alignment of $a < 0.003\,\mu$m (i.e. 30Å) silicate grains is neglected because the polarization by tiny silicate grains containing minor dust mass is negligible.

In particular, one can see from the figure that the best fit model corresponds to a peaky alignment function of PAHs with $R_{\rm peak} \approx 0.014$. Moreover, a rather low alignment degree of PAHs could be sufficient to reproduce the UV polarization feature since the mass of PAHs is dominant for the dust mass for $a < 10$Å (see Figure 3).

For HD 147933-4 (see Figure 5, lower), we find that the best fit requires no alignment of PAHs (i.e., the alignment of only silicate grains can reproduce the observed polarization). The degree of alignment $R = 0.72$ for $a > 0.15\,\mu$m silicate grains. Moreover, the alignment of silicate grains decline steeply for $a < 0.1\,\mu$m and becomes negligible ($R < 0.01$) for $a < 0.05\,\mu$m. It turns out that small silicate grains $a < 0.05\,\mu$m have minor contribution to the polarization, which is different from HD 197770. The sharp decline in alignment of small ($a < 0.1\,\mu$m) silicate grains (i.e., the polarization is dominated by larger silicate grains) is required to account for the large value of the peak wavelength $\lambda_{\rm max}$ seen in HD 147933-4.

4. POLARIZATION OF SPINNING DUST EMISSION

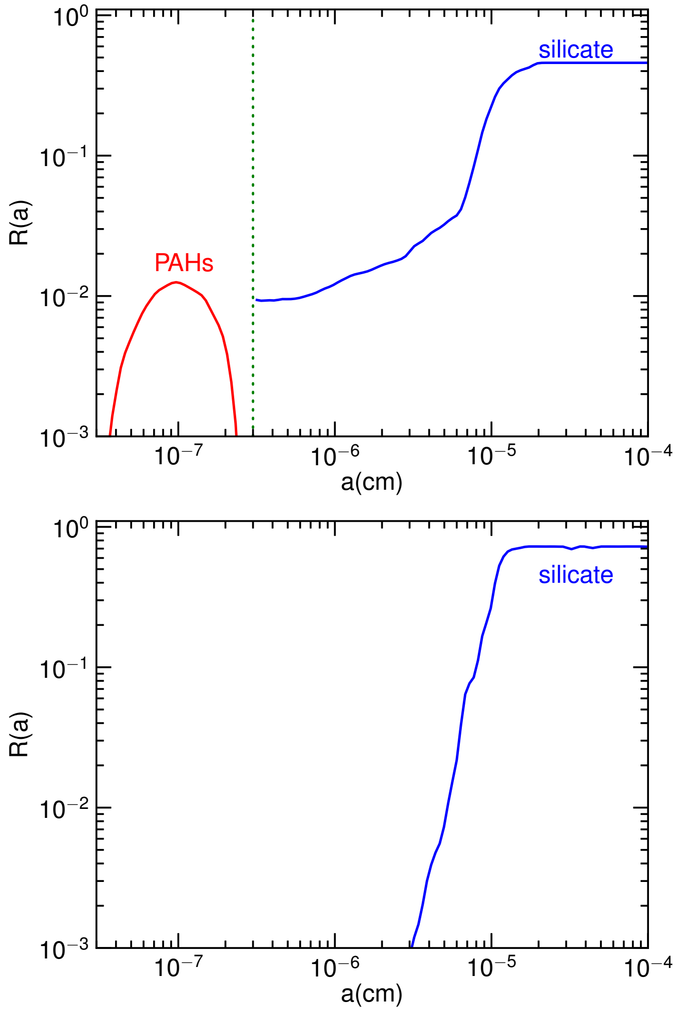

FIG. 5.— Upper panel: Degree of alignment as a function of grain size for silicate grains (blue line) and carbonaceous grains (red line) obtained from the fitting for HD 197770. Dotted line shows $a = 3 \times 10^{-7}$ cm from which the polarization by aligned small silicate grains becomes negligible. Lower panel: Similar to upper panel but for HD 147933-4. The alignment of silicate grains is shown only due to the lack of PAH alignment (see the text).

4.1. *Degree of grain alignment for spinning dust emission*

To calculate polarized spinning dust emissivity, it is important to understand the relation between the degree of alignment of PAHs that is responsible for the polarization in microwave emission and the degree of alignment of PAHs that results in starlight polarization by extinction (i.e., Rayleigh reduction factor).

As discussed in Lazarian (2007), these two measures are expected to be different. Indeed, even spherical PAHs aligned by paramagnetic mechanism can produce polarized microwave emission. Naturally, UV absorption or infrared emission is not expected from the spherical PAHs. Although we do not really believe that most of PAHs are spherical, this illustrates the problem that we face comparing different observational consequences of alignment. For instance, fast wobbling and and flipping grains are also expected to deliver substantially reduced degrees of polarization in terms of UV absorption. However, this just decreases the polarization of microwave emission by a factor of unity[5].

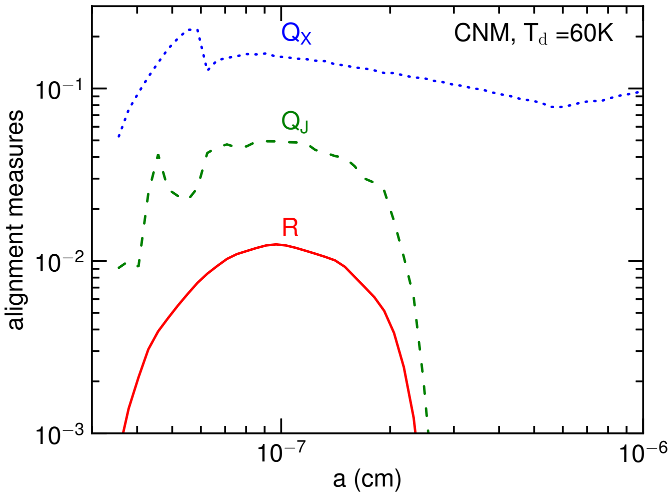

FIG. 6.— Alignment measures as functions of grain size a: Rayleigh reduction factor R, degree of alignment of grain axes with the angular momentum Q_X, and degree of alignment of angular momentum with the magnetic field Q_J.

In the following, to find the upper limit of polarized spinning dust, we adopt the degree of alignment of angular momentum with the magnetic field Q_J. Thus, from the inferred alignment function $R(a)$, we can derive Q_J using the following relationship (see Section 2.4)

$$R(a) \equiv \langle G_X G_J \rangle = Q_J \times Q_X(1 + f_{\rm corr}), \quad (19)$$

where Q_X describes the degree of alignment of grain axes with the angular momentum and $f_{\rm corr}$ describes the correlation between the internal and external alignment. The case $f_{\rm corr} = 0$ indicates that the internal alignment is independent from the external alignment. Our calculations shows that $f_{\rm corr} \sim 0.6$ for the range of size of PAHs.

Figure 6 shows the alignment measures as functions of grain size. The Rayleigh reduction factor R is from the best fit model (Figure 5, upper). Q_X is obtained from detailed calculations in Hoang et al. (2013) using Langevin equations for the cold neutral medium (CNM) and a constant dust temperature $T_{\rm d} = 60$ K. Q_J is calculated using Equation (19). It can be seen that Q_J is a factor of 3 higher than the Rayleigh reduction factor.

4.2. *Polarized spinning dust emissivity*

The polarized emissivity and unpolarized emissivity of spinning dust emission can be given by

$$q_\nu = \int Q_J(a) j_\nu(a) \frac{dn}{da} da, \quad (20)$$

$$j_\nu = \int j_\nu(a) \frac{dn}{da} da, \quad (21)$$

where $j_\nu(a)$ is the spinning dust emissivity at frequency ν from a grain of size a. The frequency dependence of polarization of spinning dust emission is $p(\nu) = q_\nu / j_\nu$. We

---

[5] One can say that for the microwave polarization from PAHs the alignment in terms of the PAH angular momenta is important, while for the UV absorption polarization, it is the alignment in terms of grain axes that is essential. The two alignments are different (see Lazarian & Roberge 1997;Hoang & Lazarian 2008; Hoang et al. 2011).

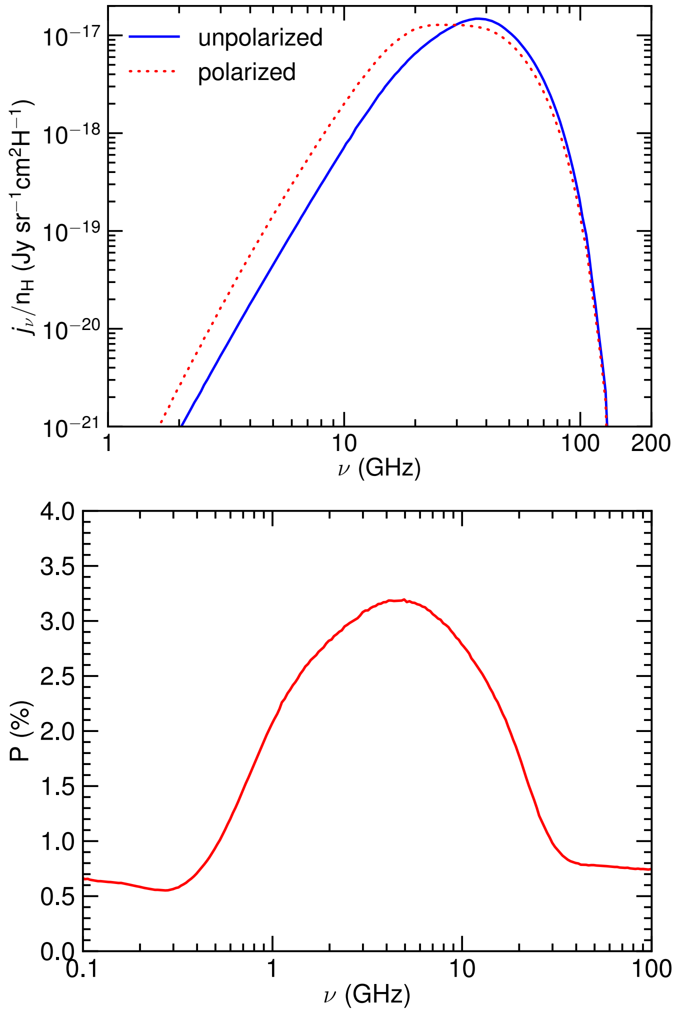

FIG. 7.— Upper panel: Unpolarized (solid line) and polarized (dotted line) spinning dust emissivity from the diffuse ISM along the line of sight to HD 197770. Lower panel: Frequency dependence of degree of polarization of spinning dust emission.

adopt the spinning dust model from Hoang et al. (2011) for oblate spheroidal grains with the ratio axis $a/b = 2$.

Figure 7 (upper panel) shows the total (unpolarized) and polarized spinning dust emissivity for the best fit model. The degree of polarization is shown in Figure 7 (lower panel). It can be seen that the maximum degree of polarization is about 3.2% and peaks at $\nu \approx 5$ GHz. The polarization is $\leq 1.8\%$ for $\nu \geq 20$ GHz.

5. DISCUSSION

In the *Planck* era, electric dipole emission from rapidly rotating PAHs has become an accepted component of diffuse galactic foreground emissions that contaminate to the CMB radiation. In light of more exciting *Planck* results on polarization, a pressing issue remains is to quantify the level of contamination by polarized spinning dust emission to the polarized CMB signal. The present paper seeks constraints on the polarization of spinning dust emission based on the models that best fit to observed polarization data of the stars having potential evidence of PAHs alignment.

5.1. *UV polarization excess and alignment of PAHs*

The polarization excess at 2175Å toward two stars, HD197770 and HD147933-4, was discovered a long time ago (Clayton et al. 1992; Wolff et al. 1993), and it is widely believed that the excess originates from aligned PAHs. Employing the observation data for these stars, we obtain the grain size distributions and alignment functions that best reproduce both the extinction and polarization curves.

For HD 197770, we found that the alignment of silicate grains only cannot reproduce the UV polarization bump adequately. Instead, a model with aligned silicate grains plus weakly aligned PAHs can successfully reproduce the UV polarization bump as well as the polarization plateau. The inferred degree of PAHs alignment present in HD 197770 varies with the grain size and has peak of 0.014 at $a \approx 9$Å. Although the degree of PAH alignment is rather small, due to the dominance of PAHs for the dust mass for $a < 20$Å, it is sufficient to reproduce the UV polarization excess. In fact, the low degree of alignment for PAHs is not unexpected from theoretical predictions based on resonance paramagnetic alignment, which was proposed by Lazarian & Draine (2000) and numerically studied in Hoang et al. 2013.

For HD 147933-4, on the other hand, we found no indication of alignment for PAHs. Yet the model with only aligned silicate grains can account for the UV polarization excess; although the model predicts a broad bump (see Figure 5).[6]

Before understanding why there is such a difference in two stars, let us recall the significant difference in optical and polarization properties of HD 197770 and HD 147933-4 (see Table 1). Indeed, the latter has a much higher ratio of visual-to-selective extinction R_V and a much larger peak wavelength $\lambda_{\rm max}$. The polarization ratio $p(2175\text{Å})/p_{\rm max}$ is much lower in the later case. Qualitatively, R_V reflects the average size of dust grains, whereas $\lambda_{\rm max}$ reflects the average size of *aligned* grains. Thus, compared to HD 197770, HD 147933-4 essentially has the larger average grain size and the larger average size of *aligned* grains. As a result, the UV polarization is dominated by the alignment of large grains. Moreover, since the large silicate grains have optical properties with oscillating features in the UV due to interference effects,[7] they can induce the broad polarization feature seen beyond $\lambda^{-1} \approx 4.6\,\mu\text{m}^{-1}$.

5.2. *Why is the UV polarization excess not seen for most stars?*

The question now is that if the PAHs are potentially aligned, why we do not see the UV polarization feature for most of stars. That answer seems straightforward. Indeed, let us consider the lines of sight of similar R_V and $\lambda_{\rm max}$. Then, the presence of UV polarization excess depends on the degree of alignment of PAHs in the ambient magnetic field. Although the alignment mechanism for PAHs is still not clear, the most promising mechanism is based on the resonance paramagnetic relaxation (LD00). Since the paramagnetic alignment is sensitive to the magnetic field and gas randomization, the variation of the magnetic field (both strength and direction) and gas density along different lines of sight can result in the absence of the UV polarization feature.

---

[6] More discussions on why it is very challenging to obtain a satisfactory fit for the UV polarization data for the stars with $\lambda_{\rm max} > 0.6\,\mu$m can be found in Kim & Martin (1995).

[7] The oscillating feature is prominent for dust with the dielectric function having small imaginary part (weakly absorbing material).

In addition, the resonance paramagnetic alignment depends on spin-spin and spin-lattice relaxation within PAHs. If the relaxation is reduced, the expected degree of grain alignment is also reduced. The point of the relaxation in PAHs, as it was claimed in LD00 can be settled via laboratory studies.

Finally, the alignment degree of PAHs in the magnetic field in general is rather weak ($R \leq 0.014$) for which the resulting UV polarization excess would be small. As pointed out in Wolff et al. (1997), this feature might not be detected by low signal-to-noise observations.

5.3. *Constraint on the polarization of spinning dust emission*

We calculated the degree of polarization for spinning dust emission using the alignment function for the best fit model to the HD 197770 data. We found that the upper limit for the polarization of spinning dust emission is $\sim 3.2\%$ at $\nu = 5\,\mathrm{GHz}$ and the degree of polarization declines rapidly to below 1.8% for $\nu > 20\,\mathrm{GHz}$.

It is worth noting that our calculations assume that the UV polarization bump is produced by PAHs only (i.e., the contribution of large graphite grains is disregarded). In fact, if graphite grains can be aligned, then their contribution to the UV polarization bump would reduce our estimate for spinning dust polarization. Therefore, this constraint is indeed the upper constraint for the spinning dust polarization.

Observationally, a number of studies indicate that anomalous microwave emission (AME) is weakly polarized (Mason et al. 2009; López-Caraballo et al. 2011). Using WMAP data, Macellari et al. (2011) found the upper limit for the polarization of AME from $1.4 - 2\%$ for $\nu = 20 - 40\,\mathrm{GHz}$. Rubiño-Martín et al. (2012) reviewed in great detail on observational constraints for the AME polarization and an upper limit of 1% for $\nu = 20-30\,\mathrm{GHz}$ is observed for the various environments. It appears that our upper limit on spinning dust polarization is consistent with the current observation data for the polarization of AME.

5.4. *Implication for polarized far-infrared thermal dust emission*

Planck Collaboration et al. (2013a) shows that the degree of polarization of thermal dust emission can reach a high level $P_{\mathrm{em}} > 15\%$ at $\nu = 353\,\mathrm{GHz}$. Let us estimate the degree of dust polarization at this frequency along the lines of sight toward two stars HD 197770 and HD 147933-4.

For simplicity, we assume that all grains have the same temperature. Thus, using the grain size distributions and alignment functions from the model, we can obtain the degree of dust polarization as follows:

$$P_{\mathrm{em}} = \frac{I_{\lambda,\mathrm{pol}}}{I_{\lambda}} \approx \frac{\sigma_{\mathrm{pol}}(\lambda)}{\sigma_{\mathrm{ext}}(\lambda)}, \tag{22}$$

where $I_{\lambda,\mathrm{pol}}$ is the polarized emission, I_{λ} is the total dust emission, and σ_{ext} and σ_{pol} are present in Equations (14) and (15).

At $\nu = 353\,\mathrm{GHz}$ (i.e., $\lambda \approx 850\,\mu\mathrm{m}$), we found the degree of polarization $P_{\mathrm{em}} = 9.9\%$ and 14.5% for HD 197770 and 147933-4, respectively. The higher degree of polarization for the HD 147933-4 star is expected because the degree of alignment of large ($a > 0.15\,\mu\mathrm{m}$) grains which dominate far-infrared dust emission is a factor of 1.55 higher than that for the HD 197770 star (see Figure 5). It can be seen that a high level of polarization ($> 15\%$) seen by *Planck* is expected from our model ($\sim 14.5\%$).

To study a potential correlation between the degree of polarization of far-infrared dust emission to that by dust extinction, we introduce a correlation parameter r, which is equal to the ratio of P_{em} at $\nu = 353\,\mathrm{GHz}$ to P_{ext}/τ at $\lambda = \lambda_{\mathrm{max}}$. We obtain $r \approx 4.7$ for HD 197770 and $r \approx 7.5$ for HD 147933-4. Interestingly, the difference in the correlation factor r of the two stars, $r(\mathrm{HD197770})/\mathrm{r}(\mathrm{HD147933-4}) = 1.59$, is close to the ratio of the degree of alignment for large grains obtained for the two stars.

6. SUMMARY

In the present paper, we obtain the constraint on the degree of polarization of spinning dust emission based on the observed extinction and polarization curves of starlight. Our principal results are summarized as follows:

1. A model of grain size distribution and alignment function for interstellar grains that best fits to the observed extinction and polarization curve is obtained for two stars HD 197770 and HD147933-4 with the prominent polarization features at 2175Å.

2. We find that a small degree of alignment (≈ 0.014) of PAHs included to the aligned silicate grains is sufficient to reproduce the UV polarization excess for HD 197770. For HD 147933-4, we find no indication of alignment for PAHs and the alignment of silicate grains can account for the excess.

3. We calculate the polarized spinning dust emission using the alignment function from the best fit model. We show that the degree of polarization for spinning dust emission has a peak of 3.2% at $\nu = 5\,\mathrm{GHz}$ and rapidly decline to below 1.8% for $\nu > 20\,\mathrm{GHz}$.

4. The degree of polarization for thermal dust emission at 353 GHz is estimated to be $P_{\mathrm{em}} = 9.9\%$ for the HD 197770 star and $P_{\mathrm{em}} = 14.5\%$ for the HD 147933-4 star.

A.L. acknowledges the financial support of the Center for Magnetic Self-Organization. T.H. thanks Brandon Hensley for useful discussions.

REFERENCES

Ali-Haïmoud, Y., Hirata, C. M., & Dickinson, C. 2009, MNRAS, 395, 1055
Bennett, C. L., Hill, R. S., Hinshaw, G., et al. 2003, ApJS, 148, 97
Bouchet, F. R., Prunet, S., & Sethi, S. K. 1999, MNRAS, 302, 663
Cardelli, J. A., Clayton, G. C., & Mathis, J. S. 1989, ApJ, 345, 245
Clayton, G. C., Anderson, C. M., Magalhaes, A. M., et al. 1992, ApJ, 385, L53
Davis, L. J., & Greenstein, J. L. 1951, ApJ, 114, 206
Dickinson, C., Davies, R. D., Allison, J. R., et al. 2009, ApJ, 690, 1585
Dolginov, A. Z., & Mitrofanov, I. G. 1976, Astrophysics and Space Science, 43, 291
Draine, B. 1989, in Interstellar Dust: Proceedings of the 135th Symposium of the International Astronomical Union, 313
Draine, B. T. 1988, ApJ, 333, 848
—. 2003, ApJ, 598, 1026
Draine, B. T., & Allaf-Akbari, K. 2006, ApJ, 652, 1318
Draine, B. T., & Flatau, P. J. 2012, arXiv, 1202, 3424
Draine, B. T., & Fraisse, A. A. 2009, ApJ, 696, 1
Draine, B. T., & Lazarian, A. 1998, ApJ, 508, 157
Draine, B. T., & Li, A. 2007, ApJ, 657, 810
Draine, B. T., & Weingartner, J. C. 1996, ApJ, 470, 551
—. 1997, ApJ, 480, 633
Efstathiou, G. 2003, MNRAS, 346, L26
Hoang, T., Draine, B. T., & Lazarian, A. 2010, ApJ, 715, 1462
Hoang, T., & Lazarian, A. 2008, MNRAS, 388, 117
—. 2009a, ApJ, 697, 1316
—. 2009b, ApJ, 695, 1457
—. 2012, Advances in Astronomy, 2012, 1
Hoang, T., Lazarian, A., & Draine, B. T. 2011, ApJ, 741, 87
Kim, S.-H., & Martin, P. G. 1995, ApJ, 444, 293
Kogut, A., Fixsen, D. J., Levin, S. M., et al. 2011, ApJ, 734, 4
Lazarian, A. 2007, J. Quant. Spectrosc. Rad. Trans., 106, 225
Lazarian, A., & Draine, B. T. 2000, ApJ, 536, L15
Lazarian, A., & Hoang, T. 2007, MNRAS, 378, 910
—. 2008, ApJ, 676, L25
Lazarian, A., & Roberge, W. G. 1997, ApJ, 484, 230
Li, A., & Draine, B. T. 2001, ApJ, 554, 778
López-Caraballo, C. H., Rubiño-Martín, J. A., Rebolo, R., & Génova-Santos, R. 2011, ApJ, 729, 25
Macellari, N., Pierpaoli, E., Dickinson, C., & Vaillancourt, J. E. 2011, MNRAS, 418, 888
Martin, P. G. 2007, in EAS Publications Series, Vol. 23, EAS Publications Series, ed. M.-A. Miville-Deschênes & F. Boulanger, 165–188
Mason, B. S., Robishaw, T., Heiles, C., Finkbeiner, D., & Dickinson, C. 2009, ApJ, 697, 1187
Planck Collaboration, Ade, P. A. R., Aghanim, N., et al. 2011, A&A, 536, A20
Planck Collaboration, Ade, P. A. R., Aghanim, N., et al. 2013a, arXiv
—. 2013b, arXiv
Roberge, W. G., & Lazarian, A. 1999, MNRAS, 305, 615
Rubiño-Martín, J. A., López-Caraballo, C. H., Génova-Santos, R., & Rebolo, R. 2012, Advances in Astronomy, 2012, 1
Serkowski, K. 1973, Interstellar Dust and Related Topics. IAU Symposium no. 52, 52, 145
Silsbee, K., Ali-Haïmoud, Y., & Hirata, C. M. 2011, MNRAS, 411, 2750
Tegmark, M., Eisenstein, D. J., Hu, W., & de Oliveira-Costa, A. 2000, ApJ, 530, 133
Tibbs, C. T., Paladini, R., Compiègne, M., et al. 2012, ApJ, 754, 94
Weingartner, J. C., & Draine, B. T. 2001, ApJ, 548, 296
Wolff, M. J., Clayton, G. C., Kim, S.-H., Martin, P. G., & Anderson, C. M. 1997, ApJ, 478, 395
Wolff, M. J., Clayton, G. C., & Meade, M. R. 1993, ApJ, 403, 722